Research Article | Vol. 32, No. 16 / 29 Jul 2024 / Optics Express 28727
Optics EXPRESS

Detection of chlorine in cement matrix using microwave-enhanced laser-induced breakdown spectroscopy

MARCUS ILLGUTH,[1] GESA KAPTEINA,[1] JOEY KIM SORIANO,[2] AND YUJI IKEDA[2,*]

[1]HafenCity Universität Hamburg (HCU), Henning-Voscherau-Platz 1, Hamburg 20457, Germany
[2]Lab., Inc., KIBC, 5-5-2, Minatojima-Minami, Chuo, Kobe, Hyogo, 6500046, Japan
[*]yuji@i-lab.net

Abstract: The detection of chloride in reinforced concrete, crucial for maintenance against damage from de-icing salt or seawater, is advanced by Laser-Induced Breakdown Spectroscopy (LIBS). This study demonstrates that integrating microwaves with LIBS enhances cement analysis, improving the signal-to-noise ratio by up to four times and extending the detection limit for chlorine to 0.17 ± 0.02 wt%. As a method, microwave-enhanced LIBS (MWE-LIBS) has existed for a decade, but in cement analysis, MWE-LIBS has been used for the first time in Cl I atomic emission measurements. This pioneering approach provides a more efficient alternative, marking a significant advancement in cement analysis.

1. Introduction

When reinforced concrete is exposed to an environment with chlorides, such as seawater or de-icing salt, the chlorides may cause severe damage and significantly reduce the service life of the structure. Chlorides can penetrate into the concrete towards the embedded reinforcement. If the chloride content at the reinforcement reaches a critical threshold of approximately 0.6% mass of cement according to the German Guideline for maintenance corrosion may start and lead to pitting corrosion resulting in large losses of the cross-section. For road structures, the expenses for maintenance and repair due to chloride-induced corrosion have increased steadily over the last years [1]. To optimize the allocation of scarce financial resources for their maintenance the knowledge of chloride distribution is important to plan maintenance and repair more efficiently.

Common methods for chloride analysis involve the analysis of concrete powder from the structure by potentiometric titration, direct potentiometry, or photometry. Usually the concrete powder is extracted directly from the structure by drilling. Sometimes also drilled concrete cores are used, which have to be further processed by cutting and/or grinding to obtain the powder. As the analyzed powder contains cement paste and aggregate the chloride content is related to the concrete mass. As threshold values linked to corrosion initiation are based on mass of cement the analyzed chloride contents have to be converted depending on the concrete composition. For existing concrete structures, the concrete composition is usually unknown, which is why estimates have to be made (usually on the safe side). This leads to the fact that although the mentioned analytic methods are precise, the results due to the sampling method might be inaccurate. By using the Laser-Induced Breakdown Spectroscopy (LIBS) technology, this uncertainty can be reduced as the aggregate can be identified and excluded from the analysis [2]. Furthermore, it is possible to achieve a deeper understanding of the spatial chloride distribution due to the much higher resolution. Due to these advantages, a guideline has recently been established in Germany [4] to enable wider application of LIBS analysis linked to chloride detection in concrete.

LIBS has been introduced as a rapid and real-time technique for chlorine detection that does not require sample preparation [5–8]. LIBS uses a focused laser beam to ablate the micro-area

#528517 https://doi.org/10.1364/OE.528517
Journal © 2024 Received 26 Apr 2024; revised 14 Jul 2024; accepted 15 Jul 2024; published 25 Jul 2024

Optics EXPRESS

of the surface of cement samples and consequently forms plasma. The ablation plasma is analyzed in a spectrometer, which separates the light by wavelength using a prism or diffraction grating to identify the elemental composition in the cement. The chlorine ions were identified at wavelengths of 134.7 nm, 479.5 nm, 593.5 nm, and 837.6 nm [9,10]. This methodology is useful for mapping cement slab layers. The LIBS method remains under scrutiny and requires significant refinement regarding its standardization of the LIBS method. However, recent inter-laboratory comparisons conducted across various countries have demonstrated high-precision measurements among different LIBS devices using identical calibration samples, effectively dispelling doubts about the methodology [11].

As LIBS gained recognition in the scientific community, its limitations became more apparent. These include the significant variability in rapid inline testing applications [12–14] and sensitivity to vibrations [15], which are particularly problematic for drone-based testing. As semiconductor microwaves achieve palm-size dimensions of 100 mm × 195 mm [16], these problems in drone-type sensors can potentially be solved with microwave-assisted LIBS. Another challenge is the reduced light transmission in optical fibers used for remote applications in areas with high radiation [17–24]. Therefore, the integration of microwave technology with LIBS is essential [25–33] to increase the plasma volume and lifetime, consequently decreasing variability, improving accuracy and repeatability in rapid in-line drone-based testing. This innovative approach has proven particularly effective in analyzing metals and oxides [34], offering substantial advantages even under high-radiation environments. The emission enhancements by microwaves are caused by localized electromagnetic radiation, resulting in increased collision rates [35], longer recombination phases [36,37], and higher production of metastable states [38,39], especially when Helium and Argon are used as ambient gases.

Microwave-enhanced LIBS, also referred to as MWE-LIBS, MW-LIBS, or MA-LIBS, is undergoing continuous development and refinement, leading to a deeper understanding of its methodology [40–42]. This approach has shown that microwave injection can expand the initial laser-induced plasma both temporally and spatially [40,41]. As a result, the plasma intensities were significantly enhanced, whereas background noise remained largely unaffected [41]. This improvement was attributed to the ability of microwaves to expand and sustain plasma ablation, demonstrating the potential for microwave enhancement in LIBS technology [42].

MWE-LIBS application in quantitative spectrochemistry has achieved numerous heights including improvements in sensitivity in detection of toxic metals in soil [43], real-time detection of Na, K and Ca during thermal conversion of biomass [44], isotope detection [45] and many other applications [46–52].

Despite these advancements, the application of microwave technology in LIBS for the analysis of cement materials remains largely unexplored, with only a few attempts to detect chlorine via calcium monochloride (CaCl) emission using molecular spectroscopy and magnetron device [53]. This study aims to bridge this gap by exploring the potential of microwave-enhanced LIBS for chlorine (Cl I) detection using quantitative atomic spectroscopy and a more advanced semiconductor microwave. In LIBS, the CaCl emission is more abundant, while Cl I is more elusive and thus more difficult to observe due to higher recombination rates and scattering in the air. Another novelty of this study is the use of a compact semiconductor helical antenna with an extended pointed tip and a cross-like plane reflector, which results in a highly concentrated localized electric field intensity compared to other antennas [31]. Such pulsed operations cannot be achieved with magnetrons. Semiconductor systems allow for precise short-pulse operations in the megahertz range and stable performance. Initial plasma generation and sustained plasma can also be produced in atmospheric air using this technology.

Our objectives were to improve the detection threshold, enhance the signal-to-noise ratio, and reduce the result variability. Enhancing the detection methodology in this manner will significantly improve the precision, efficiency, and reliability of chlorine analysis in concrete.

Optics EXPRESS

These improvements can contribute to more effective maintenance and preservation strategies for concrete structures.

2. Experimental methods

2.1. MWE-LIBS device

The LIBS experimental setup featured lasers, spectrometers, detectors, helium purge systems, and microwave systems, as shown in Fig. 1. This illustration represents the core components of the LIBS provided by Secopta FiberLIBSlab (Germany) [2]. The LIBS configuration features a diode-pumped Nd:YAG laser that operates at a wavelength of 1064 nm with a pulse frequency of 100 Hz and an energy output of 3 mJ. The setup used in previous studies [2,11]achieved a power density of approximately 39 GW/cm^2, which is necessary to generate plasma. The laser beam is focused into a spot approximately 80 micrometers in diameter using confocal mirrors with a focal length of 75 mm. The optical system was installed on a measurement head positioned 35 mm from the specimen. A schematic of the experimental setup is shown in Fig. 1.

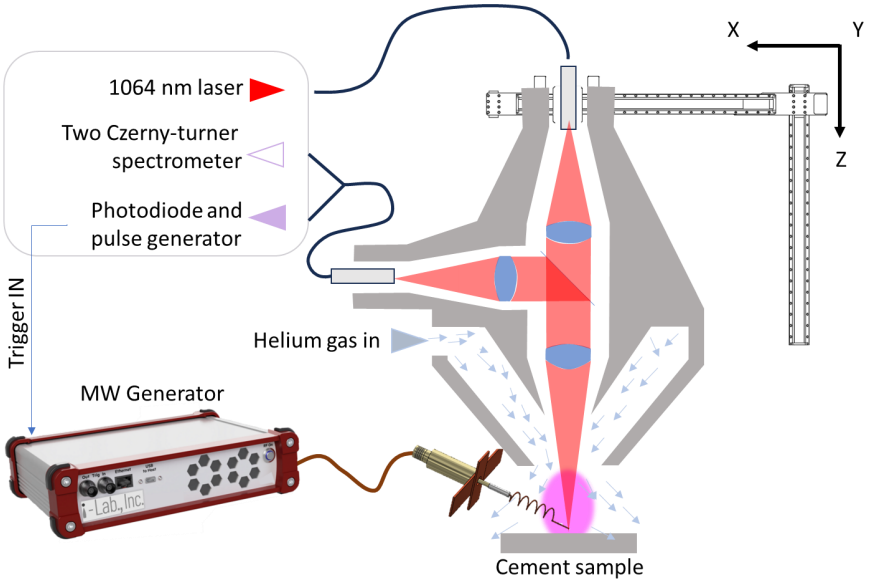

Fig. 1. The illustration of the LIBS lenses and mirrors that focuses the laser inducing ablation on the cement surface. An optical fiber sends the laser light and a second one receives the plasma light. The different beams are split by a dichroic mirror. Two Czerny-turner spectrometers are used for dispersion of light. A photodiode converts the received light into trigger signal which triggers the microwave generator. The microwave generator transmits electromagnetic energy into plasma using a helical shaped antenna (i-Lab., Inc., Japan). Note that the diagram is a conceptual representation of the LIBS and does not reflect the exact scale or the precise configuration of the optical components.

For emission signal detection, two Czerny-Turner spectrometers designed for near-infrared (NIR) and visible (VIS) light spectra were integrated to generate a wide-spectrum emission. These spectrometers feature a 1200 lines/mm grating and a 25-micrometer entrance slit (AvaSpec-ULS2048CL, Avantes, Apeldoorn, The Netherlands), covering spectral ranges of 525–750 nm for VIS and 745–940 nm for NIR, with a spectral resolution of approximately 0.1 nm. The measurement head scans the sample in 0.1 mm × 0.1 mm steps across the x and y axes, with an automated focusing mechanism on the z-axis to maintain optimal laser spot focus. This allows

Optics EXPRESS

for a two-dimensional mapping of the elemental distribution on the sample. The measurement area was flushed with helium using a 5-mm diameter tube at flowrate 10 L/min to improve measurement accuracy by eliminating interference from atmospheric gases and enhancing the atomic line visibility of chlorine at 837.6 nm.

The microwave system [56] and helical antenna designed by i-Lab Inc. (Japan) generates a 2.45 GHz microwave which induced a current with an intensified localized electromagnetic field into the laser-induced plasma [31]. The semiconductor microwave has dimensions of 23 cm × 15 cm × 5 cm. The helical antenna with an extended pointed tip and a cross-like plane reflector has a total length of 4.5 cm, with spiral part consisting of 6.5 mm diameter, coil pitch of 5 mm, The copper wire used to create the antenna has diameter of 0.5 mm. A maximum electric field strength of 2.5 MV/m is applied to the laser-induced plasma.

2.2. System operation

Figure 2 shows the synchronization of the laser, microwaves, and two spectrometers. The laser Q-switch was used to trigger both the laser and the integration time of the spectrometer. This generally eliminates the effects of the laser's jitter, as both the microwave and the spectrometer follow the laser firing. However, the trade-off is a hundred nanosecond delay between the laser and microwave/integration time caused by the photodiode. The integration time for the two Czerny-Turner spectrometers was set to 22 ms, allowing the accumulation of emissions from three consecutive laser pulses. The laser-induced plasma from the last laser pulse dissipates before 22 ms, as indicated by the photodiode signal. Consequently, the integration time was limited to 22 ms to minimize the background noise. for other number of laser shots, the integration time has to be adjusted by the following: $T = [(n-1) * 10] + 2\ ms$ [Eq. (1)]. We recognize that

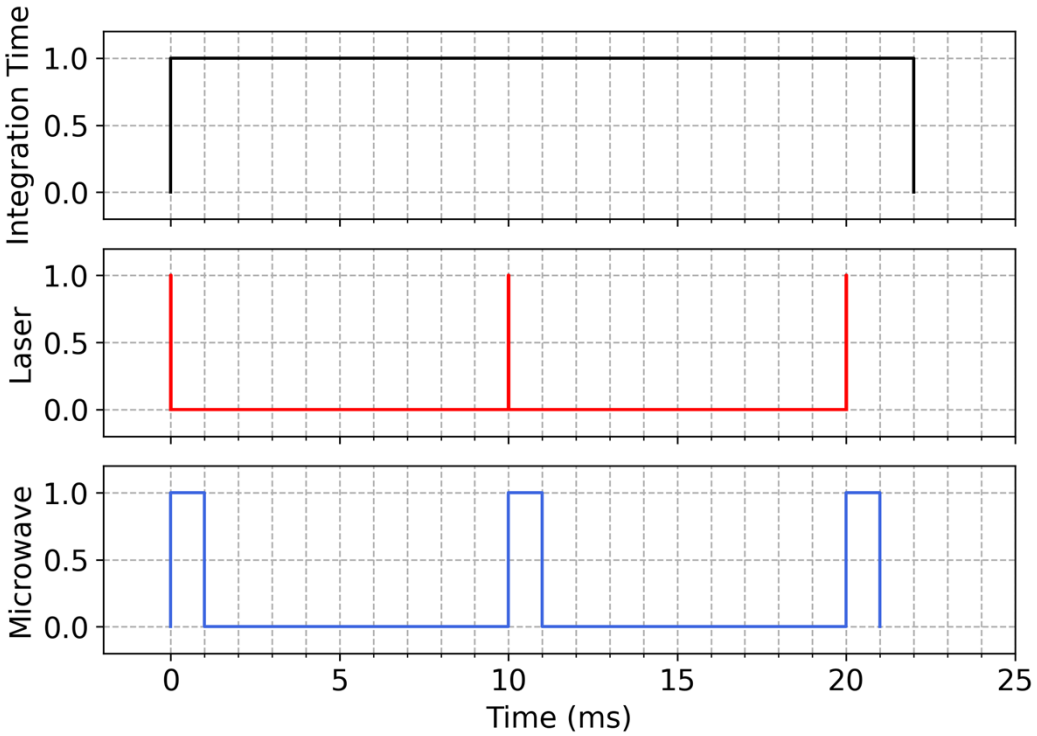

Fig. 2. Synchronization signals of the spectrometer's integration time with the laser and microwaves pulses.

Optics EXPRESS

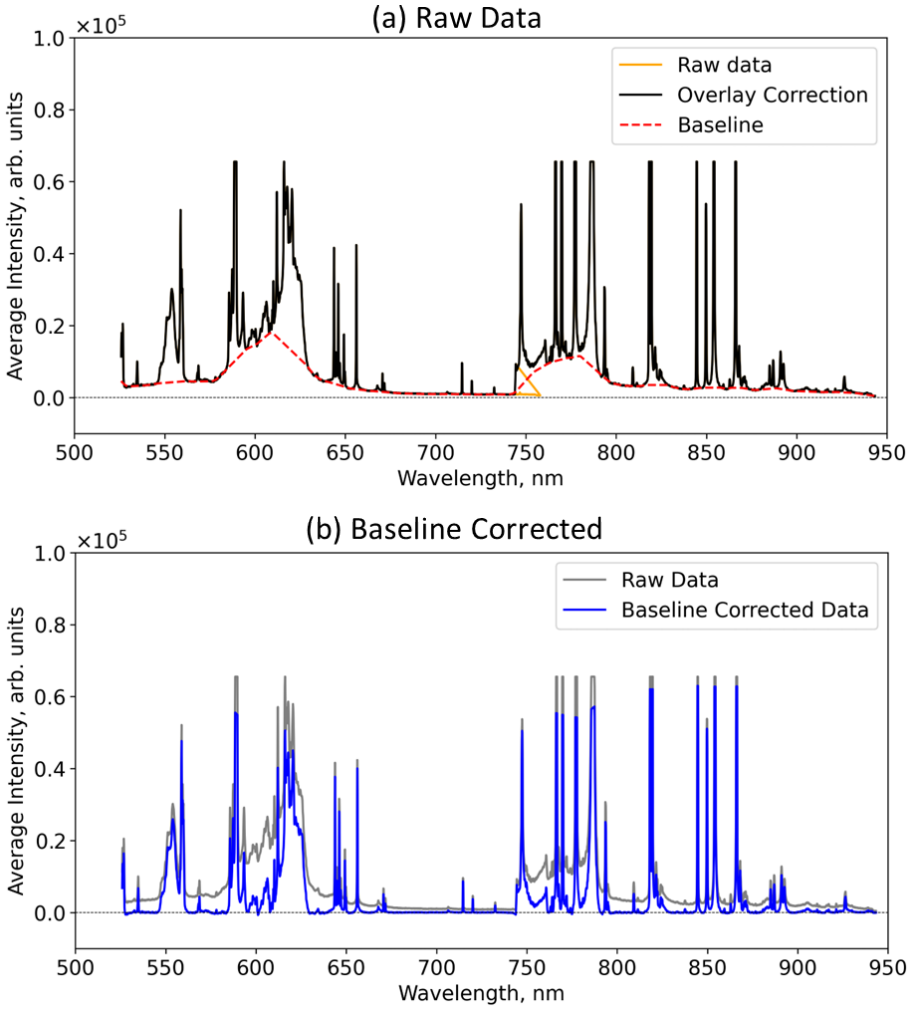

Fig. 3. Baseline correction, smoothing and sorting were necessary to remove the continuum emission in the (a) raw data resulting in a (b) baseline corrected spectrum.

this configuration will convolute significant continuum emissions caused by the Bremsstrahlung emission effect. This is a limitation of our study, which we are continuously working to improve. However, the Bremsstrahlung emission effect can be eliminated by using baseline/continuum correction.

2.3. Spectral post-processing

Secopta FiberLIBSLab implemented multiple automated signal processing techniques to subtract background signals and automate the stitching of spectra generated by two Czerny-Turner spectrometers. Despite these measures, the continuum emission from electrons necessitates further spectral processing. From the raw data shown in Fig. 3(a), the continuum emission was identified and traced using airPLS in Python, an adaptive iterative reweighted penalized least squares method for fitting the baseline spectrum. airPLS was combined with Whittaker Smooth to enhance processing [54]. Any additional signal points between 744 and 759 nm resulting from

Optics EXPRESS

the stitching of the spectra of the two Czerny Turner spectrometers were identified, sorted, and cleaned. The resulting baseline-corrected spectrum is shown in Fig. 3(b).

2.4. Cement sample preparation

Ordinary Portland cement (CEM I 42.5R) was used for the sample preparation according to DIN EN 197-1. The Cl content of each sample was adjusted by dissolving a certain amount of salt in deionized water. The Cl content was calculated based on the weight of the salt, as there are two moles of Cl per mole of salt. The cement was then mixed with water at a water/cement ratio of 0.5, filled into polyethylene bags, and sealed to minimize water loss. The samples were cured at 23°C for 28 days. They were then dried at 105 °C until they reached a constant mass. The hardened cement paste was then crushed and ground to a fine powder with a maximum particle size of approximately 90 µm. The ground powder was filled into aluminum cups and pressed into flat circular pellets (diameter = 4.0 cm, thickness = 1.0 mm). Pressing was performed at 100 N/mm^2 for 2 min.

3. Results

The enhancement effects of microwaves on the laser-induced ablation of cement were observed over a wide spectral range of 530—950 nm, as shown in Fig. 4(a). Without the microwave, the 3 mJ ablation in the Helium gas environment showed an already high emission intensity with observable Cl I emission, as shown in Fig. 4(b). At 1 kW, 1 ms pulsed microwaves were delivered into the plasma, and all emission lines increased considerably. Cl I emissions also doubled. Note that between 616 and 624 nm in the yellow-highlighted region, the CaCl molecular emissions were also significantly enhanced. However, these emissions tend to become saturated at higher Cl concentrations, rendering them unsuitable for calibration curves in the computation of the limit of detection. The spectrometer was optimized for LIBS use, which is why the emission saturation is severe with the addition of microwaves. Without the microwave addition, there are no saturated emissions. Between the CaCl, and Cl I, the CaCl is more abundant while the Cl I is more elusive to be observed. In the study by *Volker et al.* [11], both emissions can be used for quantitative analysis of Cl resulting to the same range of limit of detection (LOD) and limit of quantitation (LOQ) which are 0.02~0.10 wt% and 0.03~0.33 wt%, respectively. In the following subsections, we discuss the importance of each LIBS parameter for Cl I emission enhancement and the effects of microwaves on Cl I detection.

3.1. Importance of metastable from helium gas

One of the aims of incorporating microwaves into cement analysis is to eliminate the need for helium to observe Cl I emissions with LIBS in an air environment. Without microwave assistance, Cl I emissions were observed only with helium gas purging. In the absence of helium purging, the Cl I emission diffused, and recombination occurred rapidly, as shown in Fig. 5(a). However, microwaves offer a promising enhancement of Cl I emission with helium purging, as shown in Fig. 5(b). This enhancement is linked to a Penning-like energy-transfer process. Energy is transferred from helium atoms in a metastable excited state to Cl I atoms, similar to a bubble of energy that envelops the Cl I atom, keeping it in an excited state longer than usual. Helium in its metastable states, such as the 2^1S and 2^3S states, has an energy of 19.82 eV. When helium in this state collides with chlorine atoms, the energy transferred to chlorine can excite it to a higher energy state. This transfer occurs because the energy of the helium metastable state exceeds the excitation energy required for chlorine, which is 10.4 eV. This process prolongs and enhances the emission from chlorine. The excess energy from the helium metastable state is dissipated as kinetic energy or other forms of energy after the collision. In essence, the metastable He acts as an energizing layer, ensuring that the Cl I atom remains excited for an extended time.

Optics EXPRESS

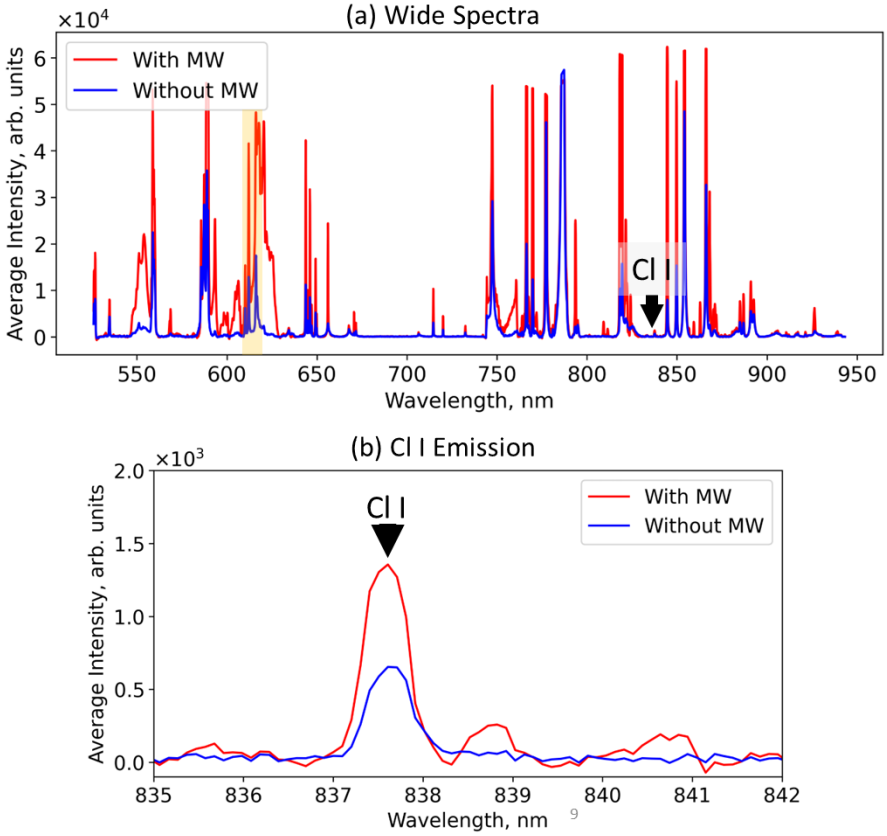

Fig. 4. (a) The wide emission spectra of the cement sample under LIBS for conditions with and without microwaves. (b) focusing on Cl I emission, the microwave enhancement is apparent using 1 kW and 1 ms pulsed microwaves.

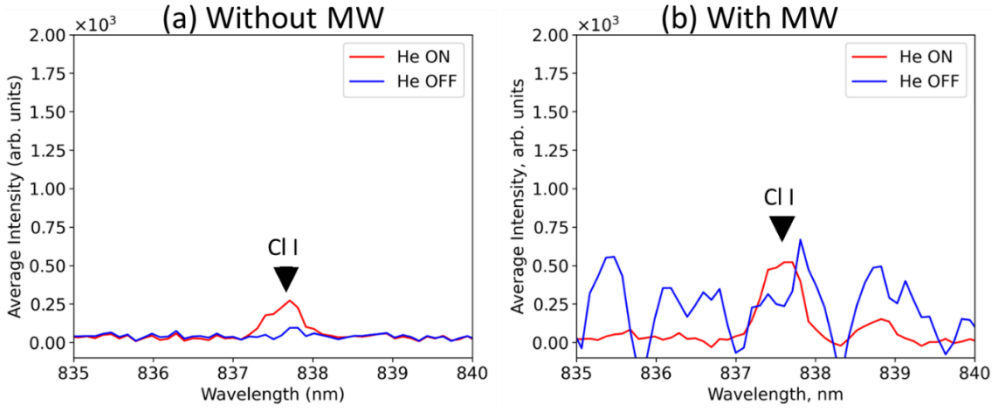

Fig. 5. The effects of Helium purging on the Cl I emission intensity using LIBS (a) without microwaves and (b) with microwaves.

Optics EXPRESS

The scenario changed when the helium purge was turned off. The Cl I emission then suffers from self-absorption, where mission peak in Cl I has a dent. This occurs because of a direct transition from the ground state when the Cl I atoms are densely packed. Without an external source of energy, this situation resembles a snow pile with a hollow peak, where the structure collapses without additional snow to bolster it. Essentially, without a secondary energy source to "keep it afloat," the emission intensity diminishes.

3.2. *Effects of laser shots*

Figure 6 shows the impact of varying the number of laser shots on the Cl I emission, with the microwave input held constant at 1 kW for and 1 ms. The enhancement of the microwave intensity effects was minimal with a single laser shot. However, this enhancement became more significant as the number of laser shots increased. This phenomenon can be attributed to the increase in the accumulated emissions resulting from the higher number of laser shots. Consequently, it is necessary to adjust and extend the integration time window to encompass all the laser shots. It means that the integration time was extended by a factor of 10 ms per laser shot.

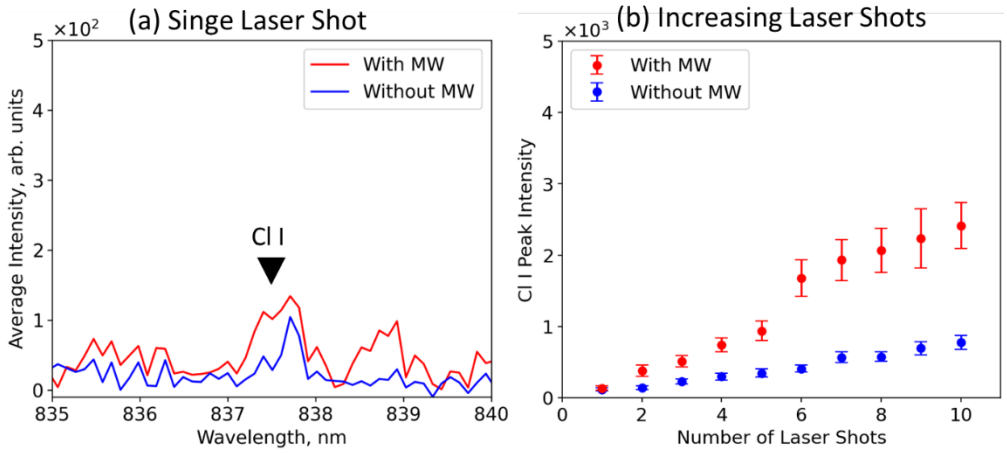

Fig. 6. Effects of (a) single laser shot and (b) increased laser shots to Cl I emission.

The same tendencies were observed for the intensity enhancement factor (IEF) and signal-to-noise ratio (SNR) with increasing numbers of laser shots as shown in Figs. 7(a) and 7(b). The IEF is a metric used to evaluate the effects of microwaves on laser-induced plasma. It is calculated by dividing the emission intensity $I_{(\lambda,MW)}$ observed when using MWE-MLIBS by the emission intensity $I_{(\lambda,LIBS)}$ from standard LIBS without microwave assistance. Mathematically, it is expressed as IEF = $I_{(\lambda,LIBS)}$ /$I_{(\lambda,MW)}$ (Eq. (2)), where $I_{(\lambda,MW)}$ is the emission intensity with microwaves and $I_{(\lambda,LIBS)}$ is the corresponding emission intensity without microwaves. As the IEF increased, the microwave effects on the plasma characteristics improved, including a higher collisional probability.

The SNR quantifies the clarity of the emission signal against the background noise. It is determined by the formula SNR = H/3σ (Eq. (3)). Here, H represents the signal height, calculated as the peak intensity (Ipeak) minus the average background signal (IBG, average), and σ is the standard deviation of the background noise. This formula provides a measure of how distinguishable the signal is from background noise.

A notable increase in intensity was observed between five and six laser shots, which was attributed to the continuous heating of the antenna, which did not cool down between experiments. In between accumulation of laser shots, there is a slight pause to the laser firing to move the laser

Optics EXPRESS

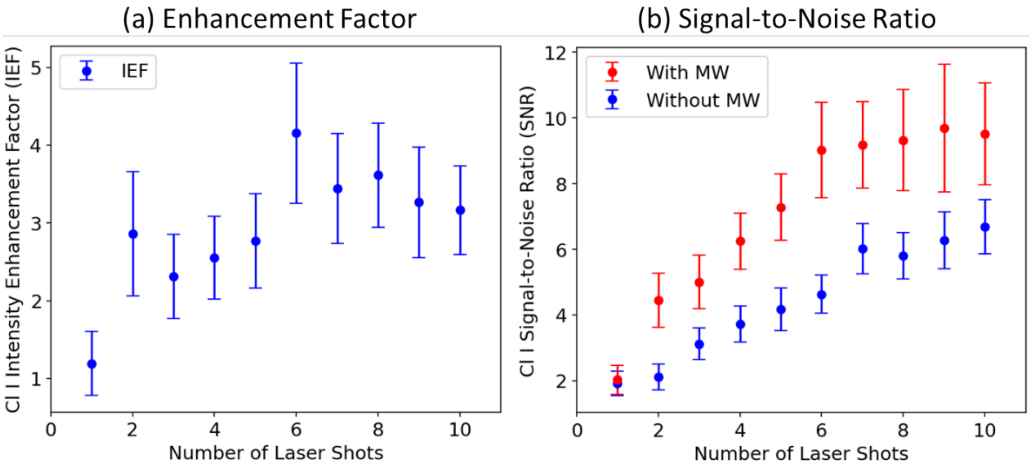

Fig. 7. (a) Intensity enhancement factor (IEF) and (Signal-to-noise Ratio (SNR) measured with increasing number of laser shots.

position from one point to another. This also helps in cooling down the antenna which worked until 5 consecutive laser shots. Using 100 Hz repetition rates, the 6-10 consecutive laser shots created more heat as also observed with the discoloration in the antenna tip. This resulted in an intensified effect of the six laser shots, analogous to the placement of metal samples on a continuously heated hot plate.

3.3. *Effects of MW parameters*

In the subsequent experiments, the number of laser shots was fixed at three to minimize variations while aiming for a high IEF and SNR. From this point onwards, antenna heating was never observed. The influence of the microwave pulse width was examined, as shown in Fig. 8. Note that the IEF significantly increased at a smaller pulse width of 200 µs and appeared to saturate at 800 µs. By contrast, the SNR displayed an approximately linear increase with the microwave pulse width, although this trend may not be definitive because of the large error margins. Accurately observing the effects of the microwave pulse width proved challenging because the 'integration time of the spectrometer was constantly set to 22 ms. This represents a limitation of the current LIBS setup, which is in the process of being upgraded. In future studies, the integration time for each microwave pulse will be adjusted.

Figure 9 shows the impact of microwave power on Cl I emissions. The IEF and SNR increased linearly with higher microwave power inputs, which can be attributed to the increased localized electromagnetic waves at higher microwave powers. However, owing to the current limitations of the LIBS setup, particularly regarding the integration time, the accuracy of the IEF and SNR measurements may not be accurately represented.

3.4. *Limit of detection*

The Limit of Detection (LOD) was derived from the calibration curves slope S of the emission signals of increasing Cl concentrations and the standard deviation σ_{blank} of the blank solution. In this study, the blank region, which lacks any emission peak between 693 to 698 nm, was utilized to calculate the σ_{blank}. The LOD equation is $LOD = 3\sigma_{blank}/S$ (Eq. (4)). This equation is commonly used for the analytical quantification of LIBS.

The calibration curve is shown in Fig. 10(a), and the LOD for both conditions, with and without microwaves, are shown in Fig. 10(b). When microwaves are utilized, the sensitivity of

Optics EXPRESS

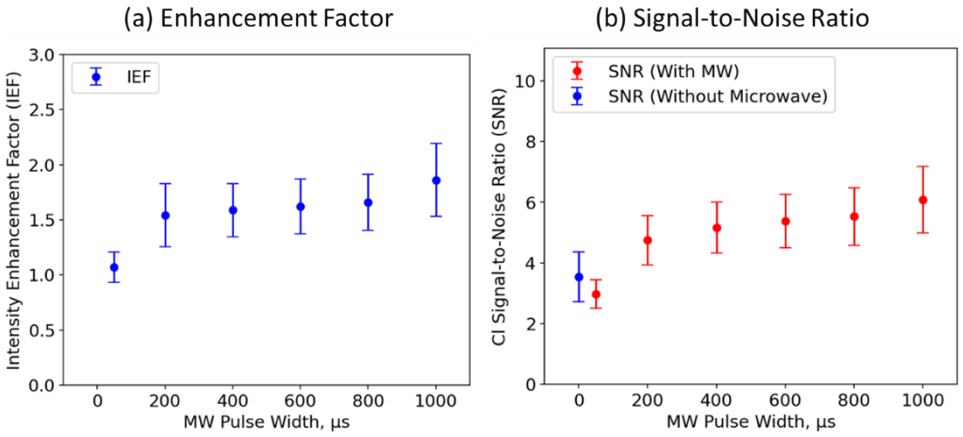

Fig. 8. (a) Intensity enhancement factor (IEF) and (Signal-to-noise Ratio (SNR) measured with increasing microwave pulse width.

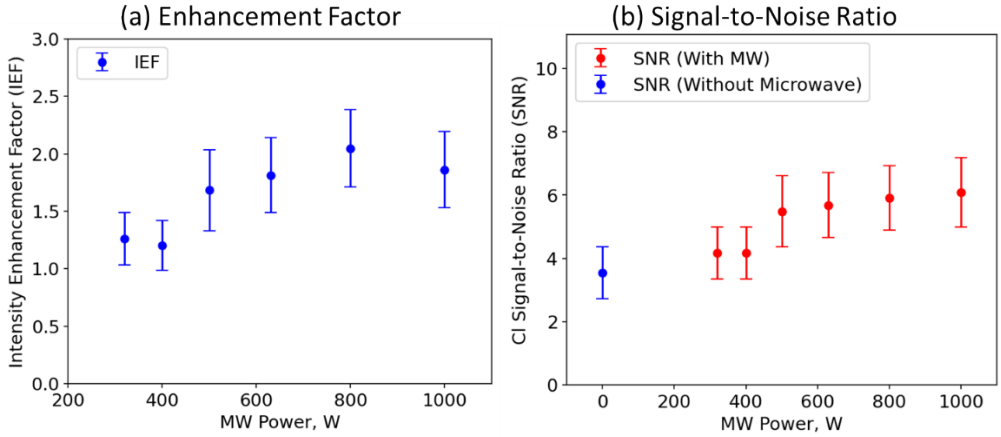

Fig. 9. (a) Intensity enhancement factor (IEF) and (Signal-to-noise Ratio (SNR) measured with increasing microwave power.

Cl I emission is notably enhanced compared to when microwaves are not used. At a maximum concentration of 0.93%, a maximum IEF of 4 and SNR of 8 were measured. The SNR was four times higher than that without microwave irradiation. However, these enhancements were accompanied by an increased variability at higher concentrations. Increased variability was also observed in the blank region, where the standard deviation of the emission-less region increased with the use of microwaves. Using Eq. (4), more pronounced slope observed under microwave conditions leads to a LOD of 0.17 wt%, significantly lower than the 0.87 wt% observed without the use of microwaves.

We acknowledge the use of various LOD computation methods, including those described in reference 11, which are similar to the German standard DIN 32645. In contrast to the method described above, this method takes into account the number of calibration and analysis measurements. For our calculation we used alpha and beta parameters set at 0.05, with a total of 1764 calibration measurements (4*441) and 441 measurements on the sample, and k = 4. The calibration samples utilized are only three, with concentrations of 0.11%, 0.20%, and 0.35%. We measured the same LOD of 0.03% under both conditions, with and without microwaves. The

Optics EXPRESS

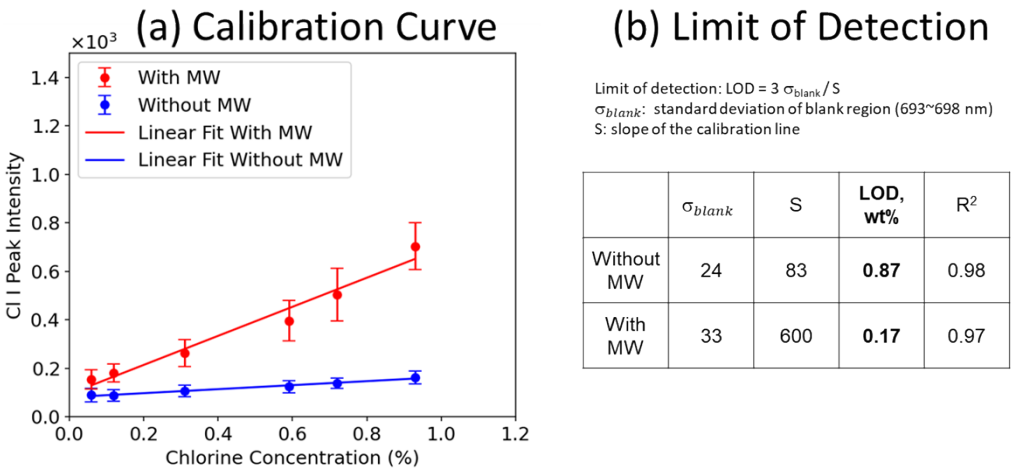

	σ_{blank}	S	LOD, wt%	R^2
Without MW	24	83	**0.87**	0.98
With MW	33	600	**0.17**	0.97

Fig. 10. (a) Calibration curve and (b) Limit of Detection (LOD) of Cl I in cement matrices with and without microwaves.

Table 1. Comparison of limit of detection (LOD) and Limit of Quantification (LOQ) of Cl I in cement matrices with other references.

	Condition	LOD/ LOQ, wt%
Standard Method	Without MW	0.87 ± 0.07 / [b]
	With MW	0.17 ± 0.02 / [b]
German standard DIN 32645[a]	Without MW	0.03 / 0.12
	With MW	0.03 / 0.11
From references	Global Interlaboratory Experiments [11]	0.01–0.10 / 0.03-0.33
	Jiaotong University, China [3]	0.19–0.26 / [b]

[a]Similar method only. The actual equation is described in reference 11.
[b]LOQ was not measured.

Limit of Quantification (LOQ) slightly decreased to 0.11% with microwave, compared to 0.12% without microwaves.

In Table 1, we compare the results with recent references. When using the standard method, the LOD improvement from 0.87 ± 0.07 wt% to 0.17 ± 0.02 wt% achieved through microwave assistance remains notably higher than the 0.01-0.10 wt% range reported in interlaboratory experiments across various countries, as listed in Table 1. The uncertainty was derived from the standard deviation of the lowest concentration. A much lower LOD at 0.0047 wt% was claimed by *Wakil et al.* [58] using MWE-LIBS on CaCl which was observed to be abundant for LIBS in the air environment. Although the repeatability of these measurements by *Wakil et al.* may be uncertain and applying the German standard DIN 32645 may also increase this value, which we aim to investigate in the future. However, the 0.17 wt % LOD fell within the range reported in [3], which employed single- and double-pulsed lasers. When using a method similar to the German standard DIN 32645 for calculating the LOD, the values fell within the expected range of 0.01–0.10 wt %. However, the use of microwaves did not significantly affect these values, and they remained stable. Nonetheless, there was a slight change in the LOQ when microwaves were used, indicating a minor increase in the measurement sensitivity with the addition of microwaves at lower Cl concentrations. As previously observed, the microwave enhancement effect was amplified at higher concentrations. The next goal was to harness this significant microwave

Optics EXPRESS

effect at the lower concentrations used in the calibration and LOD or LOQ measurements, likely through parametric optimization.

4. Discussion

An initial exploration of the role of microwaves in analyzing cement revealed both advantages and disadvantages concerning the detection of chlorine within the material. The necessary chlorine weight percentage to evaluate the quality of the cement ranges from 0.4 to 1.0% [2,3]. If the chlorine content exceeds approximately 0.6% mass of cement according to the German Guideline for maintenance corrosion, there is a recognized risk of corrosion that occurs as chloride ions infiltrate the cement, potentially reaching the reinforcing steel bars (rebars) within. This process undermines the structural integrity of cement, emphasizing the critical need for accurate chlorine level assessments to prevent corrosive damage.

The most significant and clear advantage of using microwaves in LIBS is the notable improvement in chlorine detection sensitivity. This enhancement leads to a much lower LOD compared to conventional LIBS under identical conditions with standard measurements. However, when applying a method similar to the German standard DIN 32645, the impact of microwaves becomes negligible in measuring the LOD and LOQ of chlorine at concentrations below 0.5 wt%. This is because the effect of microwaves is only pronounced at higher chlorine concentrations. If we can harness this significant microwave effect at the lower concentrations used in calibration of LOD and LOQ measurements, substantial improvements could be achieved.

A notable drawback of using microwaves in LIBS is the observed increase in variability with a higher number of laser shots and elevated chlorine concentrations. This is primarily attributed to the integration time, which must remain synchronized with the timing of the laser shots. This synchronization represents a current limitation of LIBS equipment, which is being upgraded. The impact of this limitation is also seen in saturated CaCl emission. In LIBS, the CaCl emission is more abundant, while Cl I emission is more elusive due to higher recombination rates and scattering in the air. This has been countered by He metastable through Penning-like energy transfer.

Even though this manuscript is not at par with the claimed 0.0047 wt% LOD measurements by *Wakil et al.* [53], the results contribute to a better understanding of the interaction between microwaves and Cl I. In the future, we recommend harnessing both CaCl and Cl I emissions into a multivariate calibration which could significantly improve the LOD measurements. We also recommend a decrease in integration time which may lead to reduction in variability and a decrease in saturation in CaCl with microwave use. The rationale behind this expectation is that the microwave-enhanced plasma exhibits a larger size and greater stability over extended periods. This phenomenon has been documented in previous studies [25,30,35,37,55], including the quantitative analyses of Gadolinium (Gd) in debris matrices [30].

5. Conclusions

This study explored the use of microwaves in Laser-Induced Breakdown Spectroscopy (LIBS) for cement analysis with a focus on chlorine detection. Using 3 mJ ablation in a helium gas environment already leads to high emission intensities from the cement matrix, including significant Cl I emissions. Introducing microwaves to the laser-induced plasma significantly increased all the emission lines, doubling the Cl I emissions. This is done using a compact and advanced semiconductor microwave system, and a custom design helical antenna with an extended pointed tip and a cross-like plane reflector. The results highlights the importance of helium purging, as Cl I emissions experience self-absorption without helium, indicating the need for an external energy source to maintain the emission intensity. The combined effects of increased collision probability by microwaves and Penning-like energy transfer from He

Optics EXPRESS

metastable into the Cl I resulted in the emission enhancements. The physics is slightly different from plasma confinement from external magnetic fields.

The investigation also examined the impact of changing the number of laser shots on the Cl I emissions under constant microwave conditions. An increase in the number of laser shots led to greater enhancements, indicating a strong influence on the plasma characteristics and a higher likelihood of collisions. Further analysis revealed a four-fold increase in the Intensity Enhancement Factor (IEF) and Signal-to-Noise Ratio (SNR) with more laser shots, with the possible influence of antenna heating, indicating a significant impact of microwaves on plasma properties.

Additional experiments were conducted to assess the influence of microwave parameters, particularly pulse width and microwave power, on Cl I emission enhancement. The IEF and SNR show linear increases with larger pulse widths and microwave powers despite considerable error margins owing to the fixed spectrometer integration time of 22 ms, a limitation that is planned to be addressed in future equipment upgrades.

A key achievement of this study is the significant reduction in the Limit of Detection (LOD) for chlorine in cement matrices to 0.17 wt%, a substantial improvement from the 0.87 wt% LOD observed without microwaves. However, this is still above the 0.01-0.10 wt% range reported in interlaboratory experiments. When comparing the LOD measurements with other references, the results were less favorable, particularly when compared to the claimed 0.0047 wt% LOD measurements by *Wakil et al.* using a magnetron and common-type near field applicator [58]. This result is crucial in the context of potential corrosion risks posed by chlorine levels exceeding 1.0% in cement, underscoring the importance of accurate chlorine detection to ensure structural integrity.

When using a method similar to the German standard DIN 32645 for calculating the LOD, the values fell within the expected range, but the use of microwaves did not significantly affect the LOD and Limit of Quantification (LOQ) values. This is because the effect of microwaves is only pronounced at higher chlorine concentrations.

Although integrating microwaves into LIBS offers a promising path for enhancing chlorine sensitivity and detection in cement analysis, it also introduces increased variability with a greater number of laser shots and higher chlorine concentrations. This challenge is linked to the need for synchronization between the integration time and laser shots and is anticipated to be mitigated by upgrades to the LIBS equipment. These improvements aim to reduce the variability and enhance the stability of microwave-enhanced plasma over longer durations, as supported by previous research and quantitative analyses.

Acknowledgments. The authors would like to thank the HCU for procuring the experimental equipment and for providing the staff to carry out the experiments.

Disclosures. The authors declare no conflicts of interest.

Data availability. The data underlying the results presented in this paper are not publicly available at this time but may be obtained from the authors upon reasonable request.

References

1. H. Yokota and D. Frangopol, "Bridge Maintenance, Safety, management, Life-Cycle Sustainability and Innovations," *Prodcedding of the 10th International Conference on Bridge Maintenance, Safety and Management (IABMAS 2020)*, 28th of June -2nd of July 2020, Sapporo, Japan.
2. P. Pourbozorgi Langroudi, G. Kapteina, and M. Illguth, "Automated Distinction between Cement Paste and Aggregates of Concrete Using Laser-Induced Breakdown Spectroscopy," Materials **14**(16), 4624 (2021).
3. Y. Qiu, X. Guo, M. Shi, *et al.*, "Plasma dynamics and chlorine emission characteristics on cement pastes using collinear dual-pulse laser-induced breakdown spectroscopy," Spectrochim. Acta, Part B **209**, 106799 (2023).
4. C. Bohling, D. Dalichow, C. Gottlieb, *et al.*, "Quantifizierung von Chlorid in Beton mit der laserinduzierten Plasmaspektroskopie (LIBS)," *DGZfP-Fachausschuss für Zerstörungsfreie Prüfung im Bauwesen — Unterausschuss LIBS im Bauwesen, German Society for Non-Destructive Testing*, Berlin, Germany (2023).
5. S. Millar, C. Gottlieb, T. Günther, *et al.*, "Chlorine determination in cement-bound materials with Laser-induced Breakdown Spectroscopy (LIBS) – A review and validation," Spectrochim. Acta, Part B **147**, 1–8 (2018).

Optics EXPRESS

6. S. N. Thakur and J. P. Singh, "Fundamentals of Laser Induced Breakdown Spectroscopy," in *Laser-Induced Breakdown Spectroscopy* (Elsevier, 2007), pp. 3–21.
7. A. M. Malvezzi, "Laser–Matter Interaction in LIBS Experiments," in (2014), pp. 3–29.
8. D. A. Cremers and L. J. Radziemski, "History and fundamentals of LIBS," Laser Induced Breakdown Spectroscopy: Fundamentals and Applications **1**, 1–39 (2006).
9. T. Völker, S. Millar, C. Strangfeld, *et al.*, "Identification of type of cement through laser-induced breakdown spectroscopy," Constr Build Mater **258**, 120345 (2020).
10. J. S. Cabral, C. R. Menegatti, and G. Nicolodelli, "Laser-induced breakdown spectroscopy in cementitious materials: A chronological review of cement and concrete from the last 20 years," TrAC Trends in Analytical Chemistry **160**, 116948 (2023).
11. T. Völker, G. Wilsch, I. B. Gornushkin, *et al.*, "Interlaboratory comparison for quantitative chlorine analysis in cement pastes with laser induced breakdown spectroscopy," Spectrochim. Acta, Part B **202**, 106632 (2023).
12. J. Y. Park, H. A. Kim, K. Park, *et al.*, "Rapid detection of radioactive strontium in water samples using laser-induced breakdown spectroscopy (LIBS)," Economic and Environmental Geology **50**(5), 341–352 (2017).
13. J. Qi, T. Zhang, H. Tang, *et al.*, "Rapid classification of archaeological ceramics via laser-induced breakdown spectroscopy coupled with random forest," Spectrochim. Acta, Part B **149**, 288–293 (2018).
14. R. Junjuri and M. K. Gundawar, "A low-cost LIBS detection system combined with chemometrics for rapid identification of plastic waste," Waste Manage. **117**, 48–57 (2020).
15. S. Palanco, S. Aranda, F. Mancebo, *et al.*, "Towards airborne laser-induced breakdown spectroscopy: A signal recovery method for LIBS instruments subjected to vibrations," Spectrochim. Acta, Part B **187**, 106342 (2022).
16. Y. Ikeda, "Development of 2.45 GHz semiconductor microwave system for combustion ignition enhancement and failure analysis," Materials **15**(6), 2042 (2022).
17. K. Tamura, H. Ohba, M. Saeki, *et al.*, "Development of a laser-induced breakdown spectroscopy system using a ceramic micro-laser for fiber-optic remote analysis," J. Nucl. Sci. Technol. **57**(10), 1189–1198 (2020).
18. K. Tamura, H. Ohba, M. Saeki, *et al.*, "Radiation dose rate effects on the properties of a laser-induced breakdown spectroscopy system developed using a ceramics micro-laser for fiber-optic remote analysis," J. Nucl. Sci. Technol. **58**(4), 405–415 (2021).
19. M. Saeki, A. Iwanade, C. Ito, *et al.*, "Development of a fiber-coupled laser-induced breakdown spectroscopy instrument for analysis of underwater debris in a nuclear reactor core," J. Nucl. Sci. Technol. **51**(7-8), 930–938 (2014).
20. C. Ito, H. Naito, A. Nishimura, *et al.*, "Development of radiation-resistant optical fiber for application to observation and laser spectroscopy under high radiation dose," J. Nucl. Sci. Technol. **51**(7-8), 944–950 (2014).
21. A. Matsumoto, H. Ohba, M. Toshimitsu, *et al.*, "Fiber-optic laser-induced breakdown spectroscopy of zirconium metal in air: Special features of the plasma produced by a long-pulse laser," Spectrochim. Acta, Part B **142**, 37–49 (2018).
22. M. Miyabe, M. Oba, K. Akaoka, *et al.*, "Development of laser ablation absorption spectroscopy for nuclear fuel materials: plume expansion behavior for refractory metals observed by laser-induced fluorescence imaging spectroscopy," Appl. Phys. A **126**(3), 213 (2020).
23. A. Ruas, A. Matsumoto, H. Ohba, *et al.*, "Application of laser-induced breakdown spectroscopy to zirconium in aqueous solution," Spectrochim. Acta, Part B **131**, 99–106 (2017).
24. K. Tamura, R. Nakanishi, H. Ohba, *et al.*, "Recovery of the laser-induced breakdown spectroscopy system using a ceramic microchip deteriorated by radiation for the remote elemental analysis," J. Nucl. Sci. Technol. **60**(2), 175–184 (2023).
25. Y. Ikeda, J. K. Soriano, and I. Wakaida, "Signal-to-noise ratio improvements in microwave-assisted laser-induced breakdown spectroscopy," Talanta Open **6**, 100138 (2022).
26. Y. Ikeda, J. A. Ofosu, and I. Wakaida, "Development of microwave-enhanced fibre-coupled laser-induced breakdown spectroscopy for nuclear fuel debris screening at Fukushima," Spectrochim. Acta, Part B **171**, 105933 (2020).
27. R. Nakanishi, M. Saeki, I. Wakaida, *et al.*, "Detection of Gadolinium in Surrogate Nuclear Fuel Debris Using Fiber-Optic Laser-Induced Breakdown Spectroscopy under Gamma Irradiation," Appl. Sci. **10**(24), 8985 (2020).
28. A. Khumaeni, M. Miyabe, K. Akaoka, *et al.*, "The effect of ambient gas on measurements with microwave-assisted laser-induced plasmas in MA-LIBS with relevance for the analysis of nuclear fuel," J. Radioanal. Nucl. Chem. **311**(1), 77–84 (2017).
29. Y. Ikeda, J. K. Soriano, K. Akaoka, *et al.*, "Plasma ion emission enhancements of Zr using microwave-enhanced laser-induced breakdown spectroscopy," Spectrochim. Acta, Part B **203**, 106651 (2023).
30. Y. Ikeda, J. K. Soriano, H. Ohba, *et al.*, "Analysis of gadolinium oxide using microwave-enhanced fiber-coupled micro-laser-induced breakdown spectroscopy," Sci. Rep. **13**(1), 4828 (2023).
31. Y. Ikeda, Y. Hirata, J. K. Soriano, *et al.*, "Antenna Characteristics of Helical Coil with 2.45 GHz Semiconductor Microwave for Microwave-Enhanced Laser-Induced Breakdown Spectroscopy (MW-LIBS)," Materials **15**(8), 2851 (2022).
32. Ikeda Yuji, Soriano Joey Kim, and Wakaida Ikuo, "Microwave-enhanced laser-induced breakdown spectroscopy of Zirconium metal," Talanta Open **7**(100182), 100182 (2023).
33. A. Khumaeni, T. Motonobu, A. Katsuaki, *et al.*, "Enhancement of LIBS emission using antenna-coupled microwave," Opt. Express **21**(24), 29755 (2013).

Optics EXPRESS

34. Y. Ikeda, J. K. Soriano, and I. Wakaida, "Plasma emission intensity expansion of Zr metal and Zr oxide via microwave enhancement laser-induced breakdown spectroscopy," J Anal At Spectrom **38**(6), 1275–1284 (2023).
35. M. Tampo, M. Miyabe, K. Akaoka, *et al.*, "Enhancement of intensity in microwave-assisted laser-induced breakdown spectroscopy for remote analysis of nuclear fuel recycling," J. Anal. At. Spectrom. **29**(5), 886–892 (2014).
36. Y. Ikeda and J. K. Soriano, "Analysis of the characteristics of microwave-enhanced laser-induced atmospheric air plasma and ablation plasma for Al target," Talanta Open **7**, 100172 (2023).
37. Y. Ikeda and J. K. Soriano, "Microwave-enhanced laser-induced air plasma at atmospheric pressure," Opt. Express **30**(19), 33756 (2022).
38. A. Khumaeni, K. Akaoka, M. Miyabe, *et al.*, "The role of metastable atoms in atomic excitation process of magnesium in microwave-assisted laser plasma," Opt Commun **479**, 126457 (2021).
39. R. Hedwig, I. Tanra, I. Karnadi, *et al.*, "Suppression of self-absorption effect in laser-induced breakdown spectroscopy by employing a Penning-like energy transfer process in helium ambient gas," Opt. Express **28**(7), 9259 (2020).
40. Y. Ikeda, J. K. Soriano, H. Ohba, *et al.*, *Laser Air Plasma Expansion by Microwaves* (2023).
41. Y. Ikeda, J. K. Soriano, H. Ohba, *et al.*, "Laser ablation plasma expansion using microwaves," Sci. Rep. **13**(1), 13901 (2023).
42. Y. Ikeda, J. K. Soriano, N. Kawahara, *et al.*, "Spatially and temporally resolved plasma formation on alumina target in microwave-enhanced laser-induced breakdown spectroscopy," Spectrochim. Acta Part B At. Spectrosc. **197**, 106533 (2022).
43. Y. Liu, M. Baudelet, and M. Richardson, "Elemental analysis by microwave-assisted laser-induced breakdown spectroscopy: Evaluation on ceramics," J. Anal. At. Spectrom. **25**(8), 1316–1323 (2010).
44. Y. Liu, "Improvement of the sensitivity for the measurement of copper concentrations in soil by microwave-assisted laser-induced breakdown spectroscopy," Spectrochim. Acta Part B At. Spectrosc. **73**, 89–92 (2012).
45. J. Viljanen, H. Zhao, Z. Zhang, *et al.*, "Real-time release of Na, K and Ca during thermal conversion of biomass using quantitative microwave-assisted laser-induced breakdown spectroscopy," Spectrochim. Acta Part B At. Spectrosc. **149**, 76–83 (2018).
46. A. A. Al Shuaili, A. A. Al Hadhrami, M.A. Wakil, *et al.*, "Improvement of palladium limit of detection by microwave-assisted laser-induced breakdown spectroscopy," Spectrochim. Acta Part B At. Spectrosc. **159**, 105666 (2019).
47. A. M. Alamri, J. Viljanen, P. Kwong, *et al.*, "Isotope Detection in Microwave-Assisted Laser-Induced Plasma," Plasma **6**(3), 466–477 (2023).
48. A. F. A. Kasim, M. A. Wakil, K. Grant, *et al.*, "Aqueous ruthenium detection by microwave-assisted laser-induced breakdown spectroscopy," Plasma Sci. Technol. **24**(8), 084004 (2022).
49. A. Iqbal, Z. Sun, M. Wall, *et al.*, "Sensitive elemental detection using microwave-assisted laser-induced breakdown imaging," Spectrochim. Acta Part B At. Spectrosc. **136**, 16–22 (2017).
50. J. Viljanen, Z. Sun, and Z. T. Alwahabi, "Microwave assisted laser-induced breakdown spectroscopy at ambient conditions," Spectrochim. Acta Part B At. Spectrosc. **118**, 29–36 (2016).
51. S. Wu, L. Xue, M. Yao, *et al.*, "Effect of cavity-confinement and microwave-assistance on the sensitivity of LIBS for detecting Cu content in pig feed," Optik **281**, 170800 (2023).
52. S. J. Chen, A. Iqbal, M. Wall, *et al.*, "Design and application of near-field applicators for efficient microwave-assisted laser-induced breakdown spectroscopy," J. Anal. At. Spectrom. **32**(8), 1508–1518 (2017).
53. M. A. Wakil and Z. T. Alwahabi, "Microwave-assisted laser induced breakdown molecular spectroscopy: quantitative chlorine detection," J. Anal. At. Spectrom. **34**(9), 1892–1899 (2019).
54. Z. Zhang, S. Chen, and L. Yi-Zeng, "Baseline correction using adaptive iteratively reweighted penalized least squares," Analyst **135**(5), 1138–1146 (2010).
55. Y. Ikeda, J. K. Soriano, and I. Wakaida, "The interactions of microwaves with alumina surface in microwave-enhanced laser-induced breakdown spectroscopy," Opt Laser Technol **159**, 108982 (2023).
56. Microwave enhanced system for LIBS," i-Lab, [Online]. Available: https://www.i-lab.net/english-here/new-product. [Accessed: June 2024].